



Microwave-assisted synthesis of nanosphere-like NiCo₂O₄ consisting of porous nanosheets and its application in electro-catalytic oxidation of methanol

Li Gu^a, Lei Qian^a, Ying Lei^b, Yanyan Wang^b, Jing Li^a, Hongyan Yuan^b, Dan Xiao^{a,b,*}

^aCollege of Chemistry, Sichuan University, 29 Wangjiang Road, Chengdu 610064, PR China

^bCollege of Chemical Engineering, Sichuan University, 29 Wangjiang Road, Chengdu 610064, PR China



HIGHLIGHTS

- Microwave-assisted synthesis method was used to prepare NiCo₂O₄ nanostructure.
- 3D mesoporous NiCo₂O₄ nanospheres are constructed by intertwined 2D ultrathin nanosheets.
- Nanosphere-like NiCo₂O₄ nanostructures have a large specific surface area.
- NiCo₂O₄ nanospheres exhibit high electro-catalytic activity and good long-term stability of methanol oxidation.

ARTICLE INFO

Article history:

Received 27 December 2013

Received in revised form

18 March 2014

Accepted 20 March 2014

Available online 28 March 2014

Keywords:

Microwave

Mesoporous

Nickel cobalt oxide

Nanospheres

Methanol oxidation

ABSTRACT

A fast microwave-assisted synthesis method followed by a post-calcining process is used to prepare three-dimensional (3D) nanosphere-like NiCo₂O₄ nanostructure. The 3D NiCo₂O₄ nanospheres are constructed by intertwined two-dimensional (2D) ultrathin mesoporous nanosheets. The nanosphere-like NiCo₂O₄ has a large specific surface area (SSA, 146.5 m² g⁻¹) and is successfully applied to electro-catalytic oxidation of methanol. Electrochemical impedance spectroscopy (EIS), cyclic voltammetry (CV) and chronoamperometry (CA) measurements are used to investigate electro-catalytic performance of the as-prepared NiCo₂O₄. The current density of NiCo₂O₄/Ni foam (NiCo₂O₄/NF) electrode in 1 M KOH with 0.5 M methanol is up to 40.9 A g⁻¹. And the current density can be returned to 97% of the original value by replacing new 1 M KOH electrolyte with 0.5 M methanol after a long-term CV cycle (500 cycles). These results show that our prepared NiCo₂O₄ possesses high electro-catalytic activity and good long-term stability for methanol oxidation. This may be benefit from the unique porous nanosphere-like structure and large SSA.

© 2014 Elsevier B.V. All rights reserved.

1. Introduction

The rapid depletion of fossil fuel and ever-growing environmental problems have aroused wide attention in developing and designing novel materials for electron component [1] and fuel cells [2–4]. Direct methanol fuel cells (DMFCs), as a member of fuel cells, have attracted considerable interest due to abundant raw materials, low operating temperature, high energy density as well as low pollution [5,6]. It is accepted that the relatively low activity and high cost of methanol electro-oxidation catalysts are

two main obstacles inhibiting application of DMFCs [7]. So, for DMFC anode catalyst performance improvement, the exploration of new catalyst materials including noble and non-noble metals is necessary [8]. In this respect, a number of noble metals, for instance, Pt [9,10] and Pt-based alloy [11–13], have been used as catalysts for electro-catalytic oxidation of methanol. However, high cost, self-poisoning and poor stability limit their commercial application. So, the exploration of non-noble metals with low cost and high activity is the way for catalyst cost reduction without performance compromise. Recently, transition metal oxides/hydroxides, such as NiO, [14] Co₃O₄ [15,16] and Co(OH)₂ [17], have received considerable interest due to their low cost and good electro-catalytic properties of methanol. However, poor conductivity of these metal oxides restrains their application. Therefore, in this field, it is a challenge to explore novel transition metal

* Corresponding author. College of Chemical Engineering, Sichuan University, 29 Wangjiang Road, Chengdu 610064, PR China. Tel.: +86 28 85416029; fax: +86 28 85415029.

E-mail addresses: xiaodan@scu.edu.cn, yuan_yu@scu.edu.cn (D. Xiao).

oxide catalysts with both high conductivity and electro-catalytic activity for methanol oxidation.

In recent years, as one of the transition metal oxide, NiCo_2O_4 has been widely used in supercapacitors [18,19], catalysts [20], electrochemical sensors [19], and Li-ion batteries [21] because of its intriguing advantages, such as low cost, relatively abundance and environmental friendliness [22]. Furthermore, it has been reported that NiCo_2O_4 possesses much better electronic conductivity, at least two orders of magnitude higher than nickel oxide and cobalt oxide [23]. The high electronic conductivity is favorable to the electro-catalytic activity of methanol oxidation. Although there are many reports about the applications of NiCo_2O_4 , to the best of our knowledge, the report about its application in methanol oxidation is rare [24]. Therefore, in this report, nanosphere-like NiCo_2O_4 nanostructure was proposed as a high performance catalyst for methanol oxidation.

Nowadays, there are many methods to synthesize metal oxide nano-materials, such as, hydrothermal process [25–27], sol–gel method [22,28] and electro-deposition [19,29]. Compared with the well-established approaches today, the microwave-assisted method is fast, simple and low cost, which requires less investment in equipment. Meanwhile, easy operation and short synthesis time are another two advantages for the microwave-assisted method. However, as far as we know, there were few studies on microwave-assisted method for the synthesis of NiCo_2O_4 .

In this work, a microwave-assisted method was proposed for the preparation of nanosphere-like NiCo_2O_4 structure. The as-prepared NiCo_2O_4 has been successfully applied to electro-catalytic oxidation of methanol and exhibited high electro-catalytic activity and good long-term stability.

2. Experimental

2.1. Preparation of NiCo_2O_4

Cobalt nitrate hexahydrate ($\text{Co}(\text{NO}_3)_2 \cdot 6\text{H}_2\text{O}$), nickel nitrate hexahydrate ($\text{Ni}(\text{NO}_3)_2 \cdot 6\text{H}_2\text{O}$), sodium acetate trihydrate ($\text{NaAc} \cdot 3\text{H}_2\text{O}$) and ethylene glycol (EG) were analytical grade and used as received without further purification. The experimental details were as follows. The NiCo_2O_4 prepared by a fast microwave-assisted synthesis method in addition to a post-calcining process. In a typical running, the precursor was synthesized firstly by dissolving 50 mM $\text{Ni}(\text{NO}_3)_2 \cdot 6\text{H}_2\text{O}$, 100 mM $\text{Co}(\text{NO}_3)_2 \cdot 6\text{H}_2\text{O}$ and 0.6 M $\text{NaAc} \cdot 3\text{H}_2\text{O}$ in 50 mL EG with stirring to form uniform claret solution. Then the solution was heated in a microwave oven (Panasonic, model NN-5208, Tokyo, Japan) under a medium high mode (power 560 W) for 6 min. After cooling to room temperature naturally and standing for 4 h, the solution was centrifuged at 12,000 rpm for 2 min. The supernatant was discarded and the precursor was extensively washed with distilled water and absolute ethanol several times and then dried at 80 °C in air overnight. Secondly, the precursor was calcined at 300 °C in the atmospheric environment for 2 h. After the calcination process, the precursor was converted into black powder.

2.2. Characterization of precursor and NiCo_2O_4

The scanning electron microscope (SEM) images of precursor and NiCo_2O_4 were characterized by a Hitachi S-4800 ultra-high resolution field emission scanning electron microscope (Tokyo, Japan). Transmission electron microscopy (TEM) images of NiCo_2O_4 were obtained by a FEI Tecnai G2 20 high-resolution electron microscope (Hillsboro, OR, USA). Thermogravimetric (TG) and differential thermal analysis (DTA) were carried out on a Henven HCT-2 thermal analyzer (Beijing, China) with a ramping rate of 5 °C min⁻¹

from 22 to 582 °C under a stream of air. The X-ray diffraction spectroscopy (XRD) patterns were captured by a Tongda TD-3500 X-ray power diffractometer (Liaoning, China) with $\text{Cu K}\alpha$ radiation ($\lambda = 0.15148$ nm) operating at 30.0 kV and 20.0 mA. X-ray photoelectron spectroscopy (XPS) patterns were acquired on a Kratos XSAM 800 spectrometer (Manchester, U.K.) with a $\text{Mg K}\alpha$ X-ray (1253.6 eV) excitation source running at 15 kV, and a hemispherical electron energy analyzer and multichannel detector. The Brunauer–Emmett–Teller (BET) SSA was detected by the nitrogen (N_2) adsorption method using a Quardrasorb™ SI Automated Surface Area. Fourier transform infrared spectra (FT-IR) were recorded on a Thermo Scientific Nicolet 6700 FT-IR spectrometer (Sugar Land, TX, USA).

2.3. Electrochemical measurements of $\text{NiCo}_2\text{O}_4/\text{NF}$, NiO/NF , $\text{Co}_3\text{O}_4/\text{NF}$ precursor/NF and blank NF (Blank/NF) electrodes

CV, EIS and CA measurements were implemented on an autolab electrochemical workstation (PGSTAT 30/302) to evaluate the electro-catalytic oxidation of methanol on $\text{NiCo}_2\text{O}_4/\text{NF}$ electrode. All the electrochemistry tests were carried out in a traditional three-electrode electrochemical cell with a graphite counter electrode and a Hg/HgO reference electrode, the working electrode was prepared by mixing the active materials (NiCo_2O_4 , NiO , Co_3O_4 and precursor), poly(vinylidene fluoride) and acetylene black at a weight ratio of 80:5:15 with small amount of *N*-Methyl-2-pyrrolidone (NMP). After stirring the mixture several minutes, the slurry was pasted onto NF (1.0 cm × 3.0 cm in area), which was then dried at 80 °C for 3 h. 1 M KOH without and with 0.5 M methanol were considered as electrolytes.

3. Results and discussion

The dark green precursor was originally studied by TG and DTA analysis in the temperature range of 22–582 °C to assess the follow-up calcination process. As depicted in Fig. 1, the precursor underwent two-step weight loss with a total weight loss of 27.9%. The original weight loss of 13.5% accompanied by an endothermic reaction below 130 °C is due to the removal of intercalated water molecules and physically adsorbed water molecules. Interestingly, this weight loss is much larger than that detailed in previous studies,

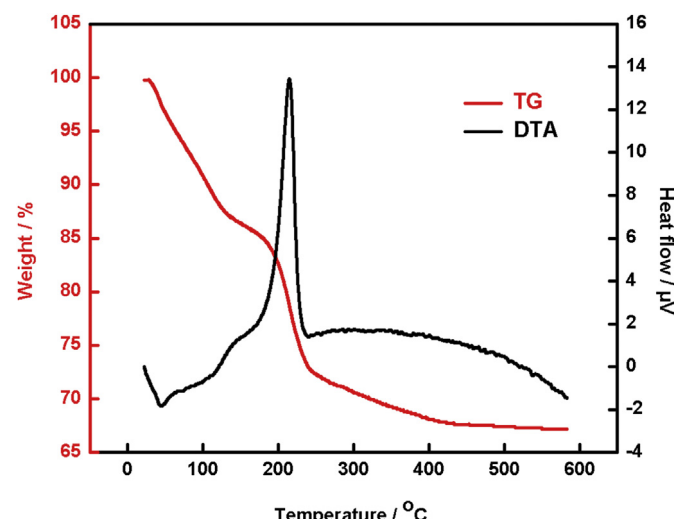


Fig. 1. TG (red) and DTA (black) curves of precursor. (For interpretation of the references to color in this figure legend, the reader is referred to the web version of this article.)

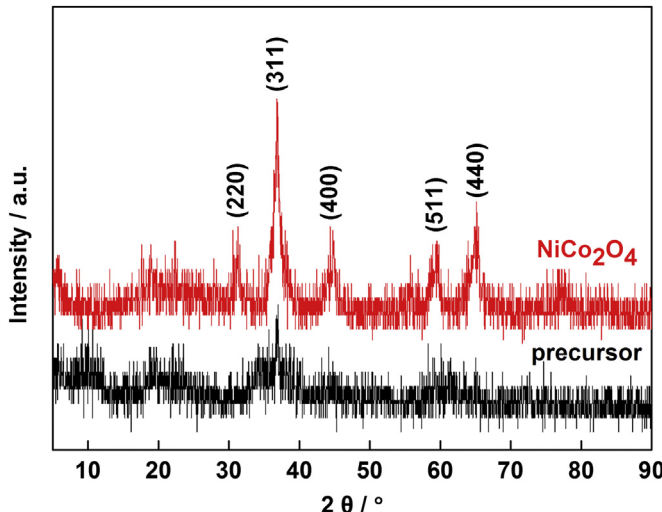


Fig. 2. XRD patterns of precursor (black) and NiCo₂O₄ (red). (For interpretation of the references to color in this figure legend, the reader is referred to the web version of this article.)

[30,31] which is usually 3–6%, inferring that our proposed precursor has large SSA or porosity to entrap the water molecules. The subsequent 14.4% weight loss with a sharp exothermic peak at 170–250 °C indicates that the precursor transformed into other species. Since the precursor is a mixture of Co(OH)₂ and Ni(OH)₂ below 130 °C, the second weight loss is ascribed to the decomposition and dehydroxylation of the hydroxide. The weight loss is a little larger than the theoretical value of 13.79% [32]. This may be due to the combustion of EG [33]. The remove of EG and intercalated water molecules may result in the destruction of precursor nanosheets, this can be found in the following SEM images (Fig. 4C and D). According to the results, 300 °C was chosen as the calcination temperature for the purpose of obtaining high purity NiCo₂O₄.

After calcination, the dark green precursor was converted into black powder, their structures and phases were characterized by XRD analysis. As shown in Fig. 2, the black curve exhibits that the precursor is a mixture of Co(OH)₂ and Ni(OH)₂, which is consistent with the previous study [34]. After calcination, the XRD pattern of the black powder (red curve) is different from the precursor (black curve), which presents five evident diffraction peaks. They coincide with the (220), (311), (400), (511) and (440) planes in the standard NiCo₂O₄ spectrum (JPCDS card No. 20-0781) perfectly. The five characteristic diffraction peaks can be indexed as the cubic spinel NiCo₂O₄. These results indicate that the NiCo₂O₄ formed after calcination process and 300 °C is appropriate for thermal conversion of precursor.

In order to demonstrate no EG molecule remained in NiCo₂O₄, we resort to FT-IR analysis. Fig. 3A depicts the FT-IR spectra of the free EG (curve a), precursor (curve b) and NiCo₂O₄ (curve c). These FT-IR spectra are clearly different. As shown in curve a, the bands at 1086 and 1043, and 2942 and 2877 cm⁻¹ are the stretching vibrations of ν_{C=O} and ν_{C-H} of the EG molecules, respectively. Compared with curve a and curve b in Fig. 3A, we can find that some EG molecules are entrapped in the precursor. After calcination (curve c), four characteristic bands of NiCo₂O₄ found at 3432, 1621, 1384, and 553 cm⁻¹ are consistent with the previous reports [35,36]. As no hydroxyl group signal of EG is detected in NiCo₂O₄, indicating that further heat treatment leads to the full decomposition of residual EG preserved in the precursor. This result is consistent with the TG-DTA analysis (Fig. 1).

To gain further information on the element composition and the oxidation state of the NiCo₂O₄, we resort to XPS measurements and the corresponding results are presented in Fig. 3B–D. By using the Gaussian fitting method, the Ni2p emission spectrum (Fig. 3B) is best fitted with one spin-orbit doublet and two shakeup satellites. One kind of Ni species has been detected and assigned to Ni²⁺. The fitting peaks at binding energy of 854.6 and 872.1 eV are indexed to Ni²⁺, [37] while the satellite peaks at 879.0 and 860.8 eV are two shake-up type peaks of the nickel at the high binding energy side of the Ni2p1/2 and Ni2p3/2 edge [38]. In the Co2p spectra (Fig. 3C),

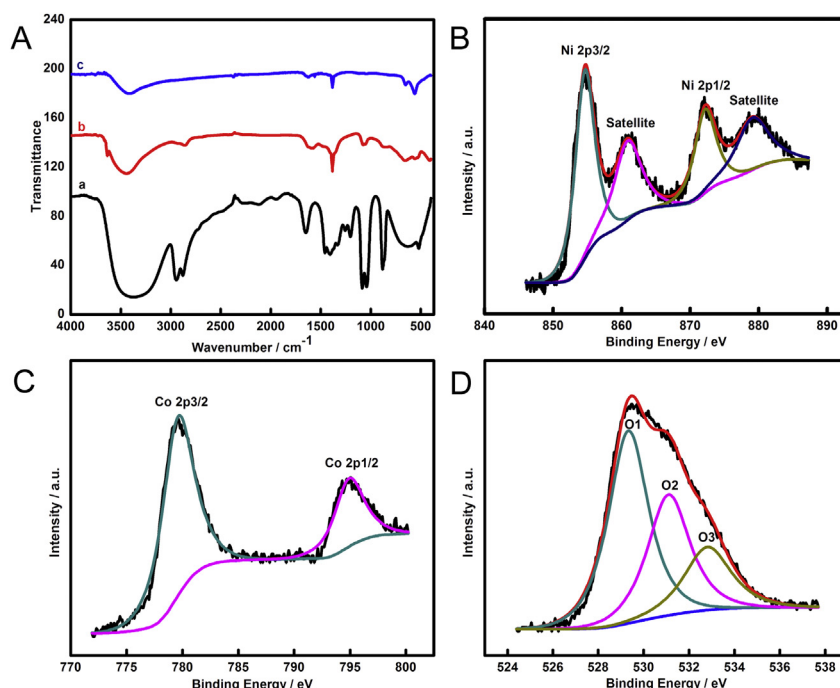


Fig. 3. (A) FT-IR spectra of (a) EG, (b) precursor and (c) NiCo₂O₄, (B) Ni2p, (C) Co2p and (D) O1s XPS spectra of NiCo₂O₄.

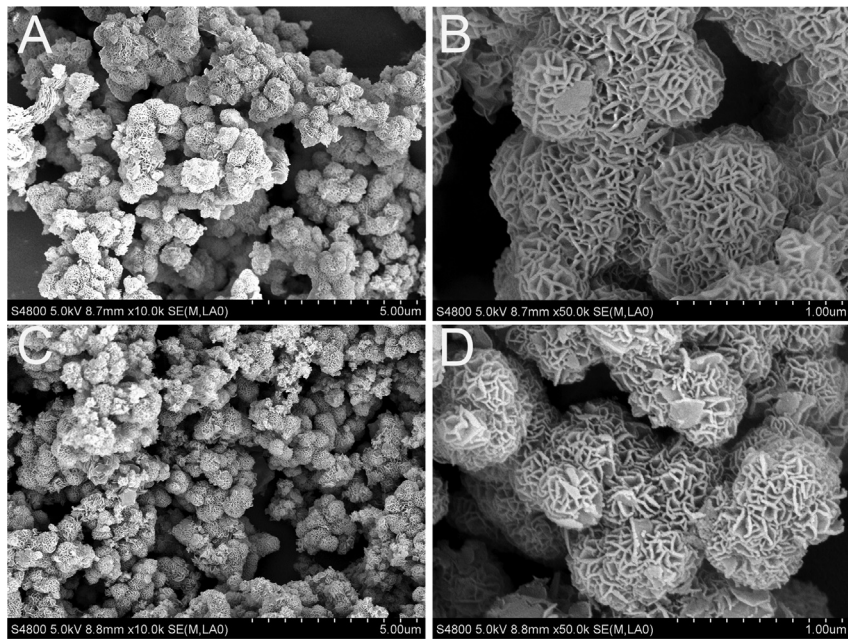


Fig. 4. SEM images of precursor (A, B) and NiCo₂O₄ (C, D).

one kind of cobalt species Co³⁺ can also be observed. The fitting peaks at 779.6 and 794.9 eV are ascribed to Co³⁺. The high-resolution spectrum for O1s region (Fig. 3D) shows three oxygen contributions, which have been denoted as O1, O2, O3, respectively. Specifically, the component O1 at 529.3 eV is typical of metal–oxygen bonds, [39] while the component O2 at 531.4 eV is associated with oxygen ions in low coordination sites at the surface [40]. The component O3 at 532.8 eV can be attributed to multiplicity of physic- and chemisorbed water at or within the surface [39]. The XPS data suggests that the surface of the prepared NiCo₂O₄ has a composition containing Co³⁺ and Ni²⁺, which could afford enough active sites for methanol oxidation.

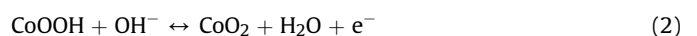
The morphology of the synthesized precursor and NiCo₂O₄ were further investigated by SEM. The SEM images are shown in Fig. 4, we can clearly see that the precursor exhibits obvious porous nanosphere-like structure (Fig. 4A), which is composed of a large number of interconnected ultrathin nanosheets (Fig. 4B). As shown in Fig. 4C and D, although the calcination process (300 °C for 2 h) causes slight destruction of nanosheets, NiCo₂O₄ still maintains the nanosphere-like structure. It is expected that this unique nanosphere-like structure might endow NiCo₂O₄ with large SSA. The intertwined feature also facilitates electrolyte penetration between NiCo₂O₄ nanosheets and charge transfer at the electrolyte-electrode interface.

TEM, high-resolution transmission electron microscopy (HRTEM) and selected area electron diffraction (SAED) were performed to further investigate the surface morphology and crystallographic structure of the proposed NiCo₂O₄. Fig. 5A is a typical TEM image of NiCo₂O₄, the black wrinkle indicates the ultrathin nanosheets structure. The blank area in the particles shows that the crinkly ultra-thin nanosheets have a porous nature. Fig. 5B shows a representative porous nanosphere-like structure of NiCo₂O₄, which assembled from ultrathin nanosheets. These results are in complete agreement with SEM results (Fig. 4C and D). The HRTEM image in Fig. 5C clearly shows that the lattice phase has random orientation. The lattice spacing of 0.25 and 0.28 nm are corresponding to the (311) and (220) planes of NiCo₂O₄, respectively. This is consistent with previous report [25]. The SAED pattern (Fig. 5D) shows well

defined rings, which is an indication of the polycrystalline nature of NiCo₂O₄. The prepared NiCo₂O₄ with such porous nanosphere-like and polycrystalline nanostructures are supposed to possess excellent electro-catalytic performance.

Distinct porous structure on the surface of NiCo₂O₄ can be viewed in SEM and TEM images. As is well known to us, the SSA is an important factor influencing the electro-catalytic performance of the materials. Therefore, the porous characteristics of as-prepared NiCo₂O₄ were further investigated by nitrogen adsorption and desorption measurements, and the results are shown in Fig. 6. The P/P_0 range of 0–0.01 suggests the micropore nature, and the hysteresis loop in the P/P_0 range of 0.4–1.0 is an indication of mesoporous structure. The N₂-adsorption isotherm of the nanosphere-like NiCo₂O₄ exhibited the combined characteristics of micropore and mesoporous, and mesoporous is in the majority. The SSA is 146.5 m² g⁻¹, which is higher than that of the previously reported NiCo₂O₄ [22,25,41]. The large SSA and porous structure not only affords enough active species for methanol oxidation but also greatly improves the electrolyte-electrode contact area, which are beneficial for a quick electrochemical reaction. Thus, the prepared NiCo₂O₄ nanostructure could provide a good activity and stability for methanol oxidation.

In order to investigate the electro-catalytic activity of our proposed NiCo₂O₄ for methanol oxidation, CV method was firstly used. As presented in curve c in Fig. 7A, the NiCo₂O₄/NF electrode exhibits one pair of redox peaks centered at 0.50 V and 0.32 V, indicating the redox reaction of NiCo₂O₄ in alkaline environment [42,43]. The redox reactions in the alkaline electrolyte are based on the following equations [44–46].



NiO and Co₃O₄ prepared by the same method were used for comparison, and the corresponding XRD results were shown in Fig. S1. We have also investigated the CV curves of precursor/NF (red curve in Fig. S2), NiO/NF, Co₃O₄/NF and Blank/NF electrodes

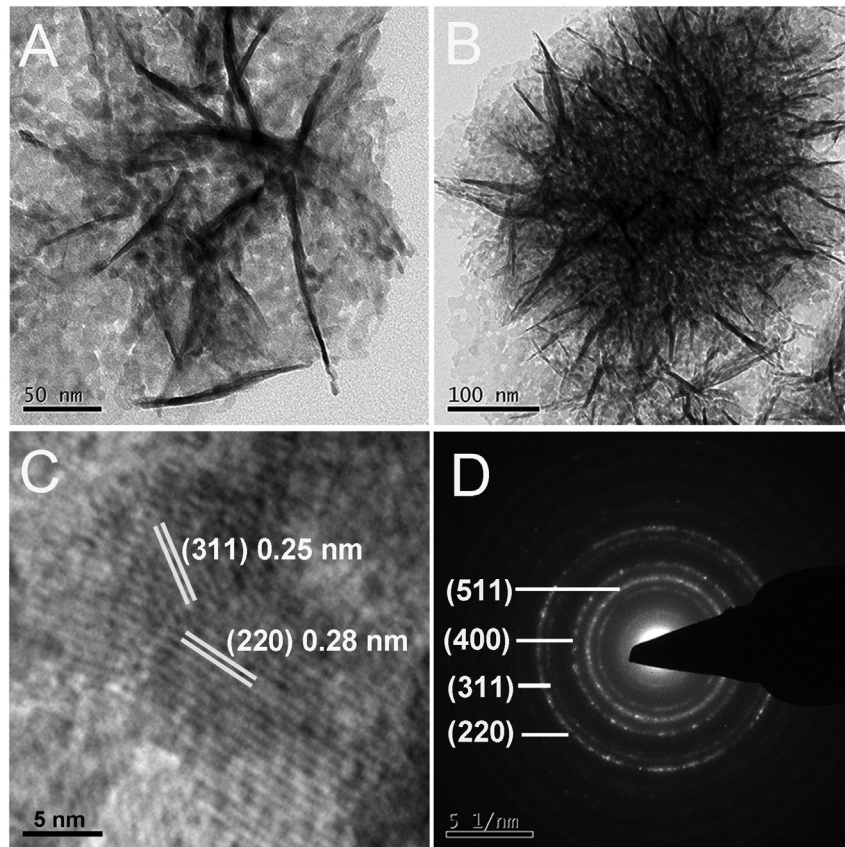
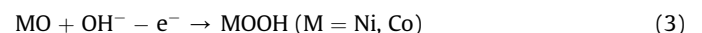


Fig. 5. TEM (A, B), HRTEM (C) and SAED (D) images of NiCo_2O_4 .

(Fig. S3) obtained at a scan rate of 10 mV s^{-1} in 1 M KOH , which are distinguished from the curve c shown in Fig. 7A. Furthermore, we investigated the electro-oxidation of methanol on $\text{NiCo}_2\text{O}_4/\text{NF}$ electrode (curve a in Fig. 7A). After addition of 0.5 M methanol in 1 M KOH , electro-oxidation of methanol on the $\text{NiCo}_2\text{O}_4/\text{NF}$ electrode is clearly observed with a sharp increase in current density at the potential over 0.37 V [47,48]. The mechanism of methanol oxidation on the $\text{NiCo}_2\text{O}_4/\text{NF}$ electrode is similar with that on the

NiO/NF and $\text{Co}_3\text{O}_4/\text{NF}$ electrodes and can be simply illustrated as follows [49–51].



The current densities of $\text{NiCo}_2\text{O}_4/\text{NF}$ in 1 M KOH without and with 0.5 M methanol are 4.6 and 40.9 A g^{-1} , respectively. These results demonstrate that the $\text{NiCo}_2\text{O}_4/\text{NF}$ electrode exhibits high activity for methanol oxidation. This high electro-oxidation activity may result from the large SSA and ultrathin mesoporous nanosheets of NiCo_2O_4 . In order to eliminate the influence of NF, the electro-catalytic activities of methanol oxidation on $\text{NiCo}_2\text{O}_4/\text{NF}$ and Blank/NF electrodes were compared. As shown in curve a and b in Fig. 7A, the $\text{NiCo}_2\text{O}_4/\text{NF}$ and Blank/NF electrodes show distinct different behavior in 1 M KOH in the presence of 0.5 M methanol. The current of $\text{NiCo}_2\text{O}_4/\text{NF}$ is much higher than that of Blank/NF, indicating the effect of blank NF on electro-catalytic oxidation of methanol can be ignored.

In order to demonstrate that the NiCo_2O_4 is favorable catalyst for methanol oxidation, the electro-catalytic activity of methanol oxidation on NiO/NF and $\text{Co}_3\text{O}_4/\text{NF}$ and precursor/NF electrodes were used for comparison in Fig. 7B. As shown in curve a, b and d in Fig. 7B, NiCo_2O_4 has much higher electro-catalytic activity for methanol oxidation than NiO and Co_3O_4 . Furthermore, the onset potential of methanol oxidation for $\text{NiCo}_2\text{O}_4/\text{NF}$ is approximately at 0.37 V (vs. Hg/HgO), much lower than that of NiO/NF and $\text{Co}_3\text{O}_4/\text{NF}$ electrodes, suggesting that the $\text{NiCo}_2\text{O}_4/\text{NF}$ electrode has much lower onset potential for direct electro-oxidation of methanol [15]. As depicted in curve c, the shape of CV curve of the precursor/NF is

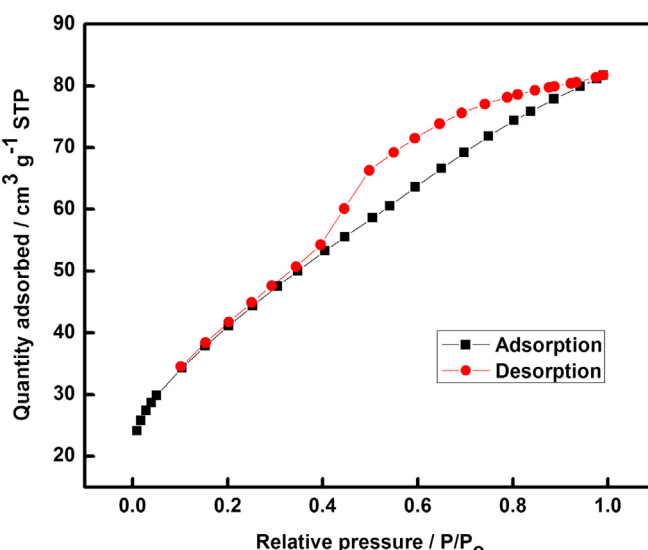


Fig. 6. N_2 adsorption–desorption isotherm loop of the NiCo_2O_4 .

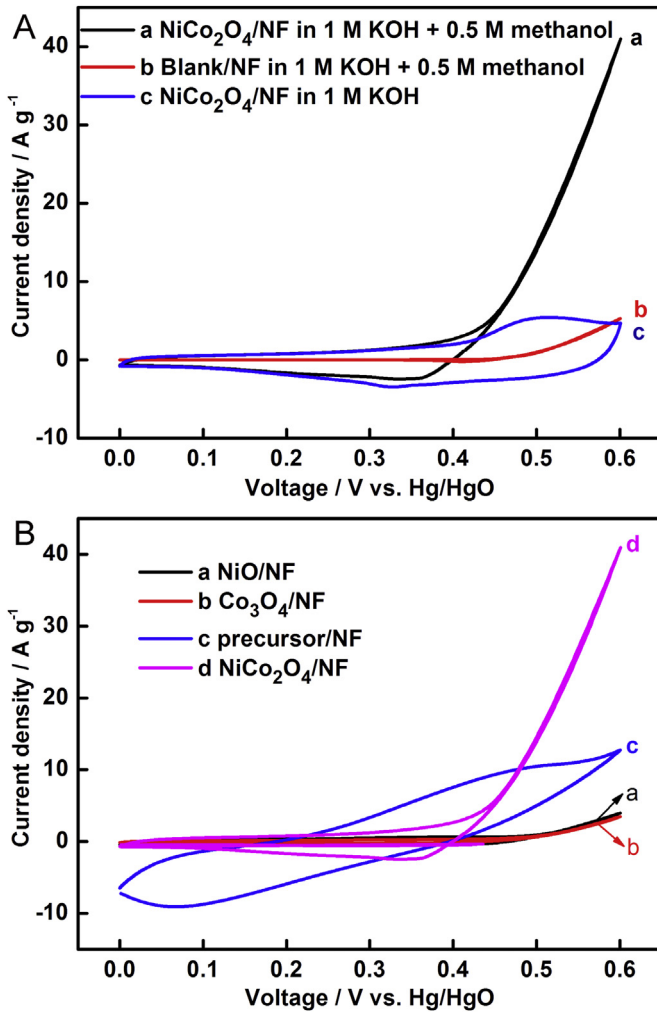


Fig. 7. (A) CV curves of NiCo₂O₄/NF in 1 M KOH without (curve c) and with (curve a) 0.5 M methanol and Blank/NF in 1 M KOH with 0.5 M methanol (curve b) at a scan rate of 10 mV s⁻¹; (B) CV curves of NiO/NF, Co₃O₄/NF, NiCo₂O₄/NF and precursor/NF in 1 M KOH with 0.5 M methanol at a scan rate of 10 mV s⁻¹.

different from the others. As shown in Fig. S2, CV curve of precursor/NF electrode in 1 M KOH with 0.5 M methanol is similar with that of precursor/NF electrode in 1 M KOH. And the current density doesn't show sharp increase after adding 0.5 M methanol, indicating that the precursor/NF electrode hardly has any electrocatalytic activity for methanol oxidation. These results demonstrate that our proposed NiCo₂O₄ have good activity for methanol oxidation and is a favorable catalyst for methanol oxidation.

EIS provides ample information for electron or charge transfer information in fuel cells reactions. Thus, EIS was carried out to further investigated methanol oxidation on NiCo₂O₄/NF. EIS measurements were recorded at 0.5 V and 0.6 V with a frequency range from 10 kHz to 0.01 Hz. The similar behavior in EIS (Fig. 8A) at 0.5 V and 0.6 V are clearly observed. However, the size of primary semicircle at 0.6 V is much smaller than that at 0.5 V, implying that the faster reaction kinetics for methanol oxidation and the lower electron or charge transfer resistance at 0.6 V [52–54]. In other way, 0.6 V is more suitable for methanol electro-oxidation.

It is well-known that CA is a useful tool to investigate the electrochemical stability of a catalyst. According to the EIS results, 0.6 V was selected as the optimal potential for investigating the stability of the Blank/NF and NiCo₂O₄/NF electrodes for methanol oxidation. As depicted in Fig. 8B, the Blank/NF and the NiCo₂O₄/NF

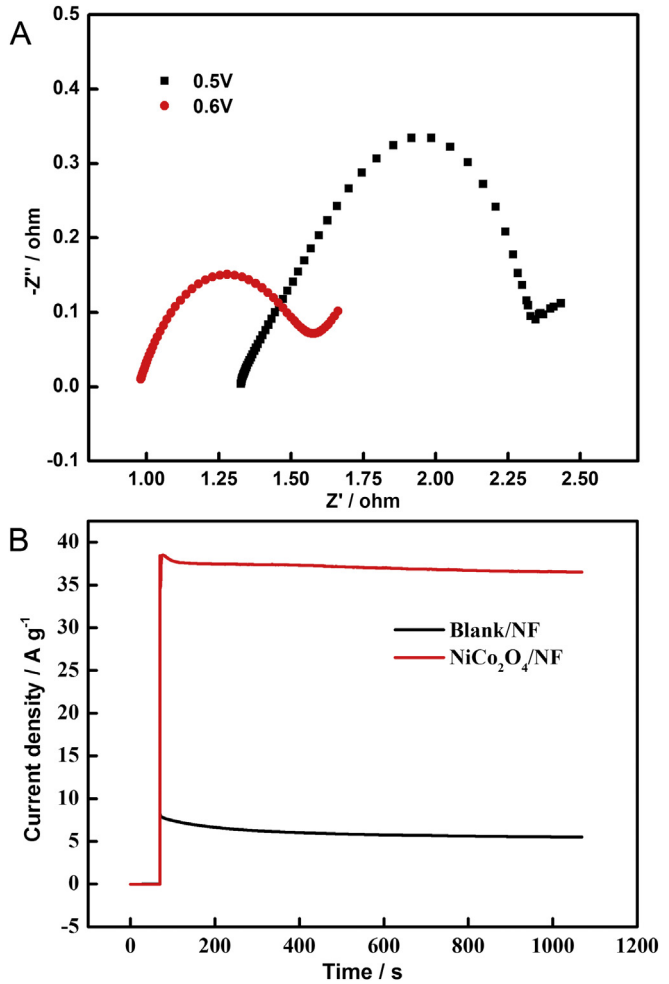


Fig. 8. (A) EIS plots of NiCo₂O₄/NF electrode in 1 M KOH with 0.5 M methanol at 0.5 V and 0.6 V. (B) CA curves of Blank/NF and NiCo₂O₄/NF electrodes in 1 M KOH with 0.5 M methanol at 0 V (0–70 s) and 0.6 V (70–1070 s).

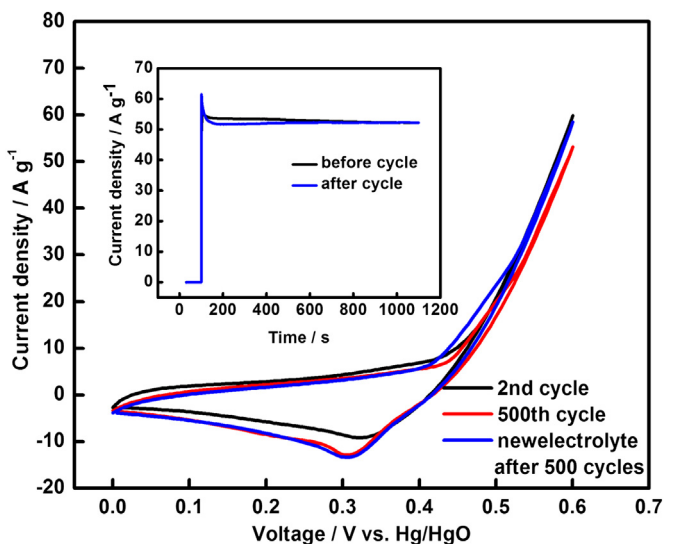


Fig. 9. CV curves of NiCo₂O₄/NF electrode measured at different cycles in 1 M KOH with 0.5 M methanol at a scan rate of 50 mV s⁻¹; inset: the CA curves of the NiCo₂O₄/NF electrode in 1 M KOH with 0.5 M methanol before (black) and after (blue) the cycle at 0 V (0–70 s) and 0.6 V (70–1070 s). (For interpretation of the references to color in this figure legend, the reader is referred to the web version of this article.)

don't show distinct decay in 1000 s, demonstrating that the NF is an ideal supporter for catalyst in DMFCs and the NiCo₂O₄/NF has good stability for methanol oxidation. Moreover, the current density of the NiCo₂O₄/NF ($\sim 37.5 \text{ A g}^{-1}$) is almost 6 times higher than that of Blank/NF ($\sim 5.2 \text{ A g}^{-1}$), which indicates that the NiCo₂O₄/NF exhibits high electro-catalytic activity of methanol oxidation and the effect of NF is too small to quantify. These are in good agreement with the CV results (Fig. 7A).

Long-term stability is another factor to assess the performance of the catalyst for the methanol oxidation. CV was used to investigate the long-term stability. As shown in Fig. 9, the current density at 0.6 V performs 89% retention after 500 cycles at a scan rate of 50 mV s⁻¹. The current density at 0.6 V can be returned to 97% of the original value by replacing the new 1 M KOH electrolyte with 0.5 M methanol. This demonstrates that the diminution of the current density with successive potential scans may probably result from the consumption of methanol. These results indicate that our proposed NiCo₂O₄ has a good long-term stability for the electro-catalytic oxidation of methanol.

To further assess the stability of the NiCo₂O₄/NF before and after 500 CV cycles, CA was employed again. As depicted in the inset image in Fig. 9, the current density of NiCo₂O₄/NF electrode after 500 CV cycles maintains 52.2 A g⁻¹ and does not show notable decay after the cycles. It is suggested that our NiCo₂O₄/NF electrode possessed high activity and good stability for methanol oxidation. This may be due to its unique 3D mesoporous nanosphere-like structure and large SSA. These results prove that NiCo₂O₄ could meet the requirements of both long-term stability and high activity, which is necessary for anodic materials in DMFCs.

4. Conclusion

In this report, a quick microwave-assisted synthesis method and post-calcination process has applied to the preparation of 3D nanosphere-like NiCo₂O₄. The mesoporous NiCo₂O₄ nanospheres has successfully used as a catalyst for methanol oxidation and displays high electro-catalytic activity and good long-term stability. The desirable electro-catalytic performance clearly indicates that the mesoporous nanosphere-like NiCo₂O₄ is a promising alternative catalyst for high performance DMFCs. These findings also demonstrate the importance and great potential of transition metal oxides in development of high-performance DMFCs.

Acknowledgments

This work was financially supported by the National Natural Science Foundation of China (Nos. 21177090, 21275104 and 21175094).

Appendix A. Supplementary data

Supplementary data related to this article can be found at <http://dx.doi.org/10.1016/j.jpowsour.2014.03.098>.

References

- [1] N.J. Curro, B.L. Young, J. Schmalian, D. Pines, Phys. Rev. B 70 (2004) 235117.
- [2] T. Hibino, A. Hashimoto, T. Inoue, J.I. Tokuno, S.I. Yoshida, M. Sano, Science 288 (2000) 2031–2033.
- [3] J.G. Liu, T.S. Zhao, R. Chen, C.W. Wong, Electrochim. Commun. 7 (2005) 288–294.
- [4] H. Mei, D.D. Andrea, T.T. Nguyen, C. Nworie, J. Power Sources 248 (2014) 1177–1180.
- [5] D. Chu, R. Jiang, Solid State Ionics 148 (2002) 591–599.
- [6] Y. Lu, J.P. Tu, C.D. Gu, X.H. Xia, X.L. Wang, S.X. Mao, J. Mater. Chem. 21 (2011) 4843–4849.
- [7] T.N. Danks, R.C.T. Slade, J.R. Varcoe, J. Mater. Chem. 12 (2002) 3371–3373.
- [8] H. Liu, C. Song, L. Zhang, J. Zhang, H. Wang, D.P. Wilkinson, J. Power Sources 155 (2006) 95–110.
- [9] Z. Wen, J. Liu, J. Li, Adv. Mater. 20 (2008) 743–747.
- [10] H. Wang, Y. Wang, Z. Zhu, A. Sapi, K. An, G. Kennedy, W.D. Michalak, G.A. Somorjai, Nano Lett. 13 (2013) 2976–2979.
- [11] X.J. Liu, C.H. Cui, M. Gong, H.H. Li, Y. Xue, F.J. Fan, S.H. Yu, Chem. Commun. 49 (2013) 8704–8706.
- [12] J. Guo, G. Sun, Q. Wang, G. Wang, Z. Zhou, S. Tang, L. Jiang, B. Zhou, Q. Xin, Carbon 44 (2006) 152–157.
- [13] S.S. Li, J.J. Lv, Y.Y. Hu, J.N. Zheng, J.R. Chen, A.J. Wang, J.J. Feng, J. Power Sources 247 (2014) 213–218.
- [14] X. Tong, Y. Qin, X. Guo, O. Moutanabbir, X. Ao, E. Pippel, L. Zhang, M. Knez, Small 8 (2012) 3390–3395.
- [15] J.B. Wu, Z.G. Li, X.H. Huang, Y. Lin, J. Power Sources 224 (2013) 1–5.
- [16] C. Xu, Z. Tian, P. Shen, S.P. Jiang, Electrochim. Acta 53 (2008) 2610–2618.
- [17] M. Jafarian, M.G. Mahjani, H. Heli, F. Gobal, H. Khajehsharifi, M.H. Hamed, Electrochim. Acta 48 (2003) 3423–3429.
- [18] H. Jiang, J. Ma, C. Li, Chem. Commun. 48 (2012) 4465–4467.
- [19] L. Huang, D. Chen, Y. Ding, S. Feng, Z.L. Wang, M. Liu, Nano Lett. 13 (2013) 3135–3139.
- [20] B. Cui, H. Lin, Y.z. Liu, J.b. Li, P. Sun, X.c. Zhao, C.-j. Liu, J. Phys. Chem. C 113 (2009) 14083–14087.
- [21] L. Zhang, S. Zhang, K. Zhang, G. Xu, X. He, S. Dong, Z. Liu, C. Huang, L. Gu, G. Cui, Chem. Commun. 49 (2013) 3540–3542.
- [22] T.Y. Wei, C.H. Chen, H.C. Chien, S.Y. Lu, C.C. Hu, Adv. Mater. 22 (2010) 347–351.
- [23] Y. Li, P. Hasin, Y. Wu, Adv. Mater. 22 (2010) 1926–1929.
- [24] L. Qian, L. Gu, L. Yang, H.Y. Yuan, D. Xiao, Nanoscale 5 (2013) 7388–7396.
- [25] H. Wang, Q. Gao, L. Jiang, Small 7 (2011) 2454–2459.
- [26] H. Wan, X. Ji, J. Jiang, J. Yu, L. Miao, L. Zhang, S. Bie, H. Chen, Y. Ruan, J. Power Sources 243 (2013) 396–402.
- [27] X.A. Chen, X. Chen, F. Zhang, Z. Yang, S.M. Huang, J. Power Sources 243 (2013) 555–561.
- [28] K. Shimamoto, K. Tadanaga, M. Tatsumisago, J. Power Sources 248 (2014) 396–399.
- [29] Z. Quan, S. Ohguchi, M. Kawase, H. Tanimura, N. Sonoyama, J. Power Sources 244 (2013) 375–381.
- [30] C. Jin, F. Lu, X. Cao, Z. Yang, R. Yang, J. Mater. Chem. A 1 (2013) 12170–12177.
- [31] B. Chi, J. Li, Y. Han, Y. Chen, Int. J. Hydrogen Energy 29 (2004) 605–610.
- [32] B. Cui, H. Lin, J.B. Li, X. Li, J. Yang, J. Tao, Adv. Funct. Mater. 18 (2008) 1440–1447.
- [33] X. Tian, C. Cheng, L. Qian, B. Zheng, H. Yuan, S. Xie, D. Xiao, M.M.F. Choi, J. Mater. Chem. 22 (2012) 8029–8035.
- [34] C.C. Hu, C.T. Hsu, K.H. Chang, H.Y. Hsu, J. Power Sources 238 (2013) 180–189.
- [35] X. Wang, W.S. Liu, X. Lu, P.S. Lee, J. Mater. Chem. 22 (2012) 23114–23119.
- [36] S. Verma, H.M. Joshi, T. Jagadale, A. Chawla, R. Chandra, S. Ogale, J. Phys. Chem. C 112 (2008) 15106–15112.
- [37] Z.Q. Liu, Q.Z. Xu, J.Y. Wang, N. Li, S.H. Guo, Y.Z. Su, H.J. Wang, J.H. Zhang, S. Chen, Int. J. Hydrogen Energy 38 (2013) 6657–6662.
- [38] J. Xiao, S. Yang, J. Mater. Chem. 22 (2012) 12253–12262.
- [39] J.F. Marco, J.R. Gancedo, M. Gracia, J.L. Gautier, E. Rios, F.J. Berry, J. Solid. State. Chem. 153 (2000) 74–81.
- [40] Y.E. Roginskaya, O.V. Morozova, E.N. Lubnin, Y.E. Ulitina, G.V. Lopukhova, S. Trasatti, Langmuir 13 (1997) 4621–4627.
- [41] M. Cabo, E. Pellicer, E. Rossinyol, M. Estrader, A. Lopez-Ortega, J. Nogues, O. Castell, S. Surinach, M.D. Baro, J. Mater. Chem. 20 (2010) 7021–7028.
- [42] R. Ding, L. Qi, M. Jia, H. Wang, Nanoscale 6 (2014) 1369–1376.
- [43] X.Y. Liu, Y.Q. Zhang, X.H. Xia, S.J. Shi, Y. Lu, X.L. Wang, C.D. Gu, J.P. Tu, J. Power Sources 239 (2013) 157–163.
- [44] G. Hu, C. Tang, C. Li, H. Li, Y. Wang, H. Gong, J. Electrochem. Soc. 158 (2011) A695–A699.
- [45] V. Gupta, S. Gupta, N. Miura, J. Power Sources 175 (2008) 680–685.
- [46] X. Wang, X. Han, M. Lim, N. Singh, C.L. Gan, M. Jan, P.S. Lee, J. Phys. Chem. C 116 (2012) 12448–12454.
- [47] Q. Yi, W. Huang, J. Zhang, X. Liu, L. Li, Catal. Commun. 9 (2008) 2053–2058.
- [48] N. Laosiripojana, S. Assabumrungrat, J. Power Sources 163 (2007) 943–951.
- [49] M. Asgari, M.G. Maragheh, R. Davarkhah, E. Lohrasbi, J. Electrochim. Soc. 158 (2011) K225–K229.
- [50] N. Spinner, W.E. Mustain, Electrochim. Acta 56 (2011) 5656–5666.
- [51] H. Heli, H. Yadegari, Electrochim. Acta 55 (2010) 2139–2148.
- [52] Y.p. Gan, H. Huang, W.K. Zhang, Trans. Nonferrous Met. Soc. China 17 (2007) 214–219.
- [53] S.S. Mahapatra, A. Dutta, J. Datta, Int. J. Hydrogen Energy 36 (2011) 14873–14883.
- [54] H. Wang, J. Du, Z. Yao, R. Yue, C. Zhai, F. Jiang, Y. Du, C. Wang, P. Yang, Colloids Surf. A 436 (2013) 57–61.